New Journal of Physics
The open access journal at the forefront of physics

PAPER • OPEN ACCESS

Multiple ionic memories in asymmetric nanochannels revealed by mem-spectrometry

To cite this article: Simon Jouveshomme *et al* 2025 *New J. Phys.* **27** 065001

IOP Publishing New J. Phys. 27 (2025) 065001 https://doi.org/10.1088/1367-2630/ade61b

New Journal of Physics
The open access journal at the forefront of physics

Deutsche Physikalische Gesellschaft DPG
IOP Institute of Physics

Published in partnership with: Deutsche Physikalische Gesellschaft and the Institute of Physics

OPEN ACCESS

RECEIVED
17 April 2025

REVISED
10 June 2025

ACCEPTED FOR PUBLICATION
19 June 2025

PUBLISHED
26 June 2025

PAPER

Multiple ionic memories in asymmetric nanochannels revealed by mem-spectrometry

Simon Jouveshomme[1], **Mathieu Lizée**[1,3], **Paul Robin**[2] **and Lydéric Bocquet**[1,*]

[1] Laboratoire de Physique de l'École normale supérieure, Centre national de la Recherche scientifique, Paris, France
[2] Institute of Science and Technology Austria, Am Campus 1. 3400, Klosterneuburg, Austria
[3] Current address: Fritz Haber Institute of the Max Planck Society, Berlin, Germany.
[*] Author to whom any correspondence should be addressed.

E-mail: lyderic.bocquet@ens.fr

Keywords: memristor, iontronics, nanofluidics, nanopores

Abstract

Recently discovered nanofluidic memristors, have raised promises for the development of iontronics and neuromorphic computing with ions. Ionic memory effects are related to ion dynamics inside nanochannels, with timescales associated with the manifold physicochemical phenomena occurring at confined interfaces. Here, we explore experimentally the frequency-dependent current–voltage response of model nanochannels—namely glass nanopipettes—to investigate memory effects in ion transport. This characterisation, which we refer to as mem-spectrometry, highlights two characteristic frequencies, associated with short and long timescales of the order of 50 ms and 50 s in the present system. Whereas the former can be associated with ionic diffusion, very long timescales are difficult to explain with conventional transport phenomena. We develop a minimal model accounting for these mem-spectrometry results, pointing to surface charge regulation and ionic adsorption-desorption as possible origins for the long-term memory. Our work demonstrates the relevance of mem-spectrometry to highlight subtle ion transport properties in nanochannels, giving hereby new insights on the mechanisms governing ion transport and current rectification in charged conical nanopores.

1. Introduction

Ion transport through solid-state nanochannels exhibits rich properties [1–3], including anomalously high conductivity [4–9], ionic selectivity [10–14], ionic current rectification [15–31], non-monotonous current–voltage relations [32–37] and mechanosensitivity [38, 39]. These original transport properties of confined electrolytes might be used to interface biological living systems [40, 41], or implement neuromorphic computing [42, 43]. So far, ionic diodes, transistors [44–46] and triodes [47, 48] were demonstrated, and nanofluidic components were used to implement various computational tasks [43, 49].

Among other components, the so-called nanofluidic memristors (short for memory resistors), characterised by history-dependent conductances, have aroused a lot of attention [43, 50–57], since they are promising elements for mimicking biological synapses, building circuits combining computation and memory module in a single unit, for complex signal processing [58] or as non-linear components in dynamical systems [56]. The conductance of a memristor depends on its internal microscopic state (for example, ion concentration inside the device). The latter varies depending on the applied voltage drop ΔV, leading the conductance to evolve over time, converging to the equilibrium value $G_\infty(\Delta V)$. In a wide class of nanofluidic memristors functioning with voltage-driven ionic accumulation/depletion, the conductance evolution was predicted to occur over a typical timescale τ, referred to as the memory time of the memristor, and roughly equal to the diffusion time of ions through the device [52, 54, 56], which is of the order of 100 ms for a nanofluidic device of length $L \approx 10\,\mu$m. This estimate is consistent with some experimental results [49, 54, 58, 59] but more subtle behaviour were reported as well. In particular, complex memory effects were reported in nanofluidic devices, such as long-term potentiation in 2D nanochannels (after a bias pulse, the

conductance quickly relaxes to a value close to the initial value, but remains higher than original value for a long time) [54], or an analysis of conductivity evolution involving two characteristic times in functionalised charged conical nanopore [55], for which a clear understanding is lacking.

In the present work, we explore more thoroughly how the channel's memory depends on the excitation frequency, a technique which may be coined mem-spectrometry. Anticipating on the result to be shown below, this mem-spectrometry approach highlights two different characteristic frequencies, associated with a short ($\tau_{\rm fast} \approx 50$ ms) and a long ($\tau_{\rm slow} \approx 50$ s) time scales for the ionic dynamic in glass nanopipettes. We characterise how these typical timescales depend on electrolyte concentration, and show that long-term memory fades at high concentration, while the short-term memory is shifted towards higher frequencies. Finally, we discuss several scenarios accounting for the emergence of two separate time-scales in asymmetrical channels.

The present article is organised as follows: first we characterise our nanopipettes, and show that ion transport exhibits memory effects, in the sense that the conductance of the pipette depends on the history of applied voltage. Then, using mem-spectroscopy, we report the frequency and amplitude of the memory effect as a function of salt concentration. Finally, we introduce a minimal model involving the dynamics of surface charges which qualitatively accounts for our results.

2. Materials and methods

We carry out measurements on three nanopipettes, obtained from quartz capillaries, which display the same tip radii of 50 ± 15 nm (see SEM image in figure 1(a)). Before filling a pipette with a solution, we expose it to an oxygen plasma for ten minutes to ensure a clean and hydrophilic surface. We prepare KCl electrolytes with MiliQ deionised water (resistivity of 18.2 MΩcm at 25°C) and KCl crystal (Sigma-Aldrich, purity $\geqslant 99.5\%$) with varying concentration c. pH is fixed at 5 by adding HCl salt in proportion $[\mathrm{HCl}] = 10^{-5}\,\mathrm{M} \ll [\mathrm{KCl}]$.

Our experimental setup for ionic current measurement is sketched in figure 1(b). The pipette is immersed in the electrolyte, its tip separating the fluid into two reservoirs, corresponding to the inside and the outside of the pipette. We insert one Ag/AgCl electrode in both reservoirs, and link them to a patch-clamp amplifier (Axopatch-200B), which we used to impose time-dependent sinusoidal voltage with varying frequencies f, and to record the induced ionic current. As many charged conical nanopores, glass nanopipettes are well-known for rectifying ionic current [15, 20, 21, 30, 39], thus behaving like ionic diodes. When the bias causes the counterions to move from the tip to the base of the pipette, the ion concentration increases near the tip, resulting in a high conductance. Conversely, reversing the bias results in a depletion of ions near the tip which lowers conductance.

We measure the IV characteristics under quasi-constant bias, as the one shown in figure 2(a), and report a drop of rectification ratio (ratio of conductance at 1 V and −1 V) with ionic concentration, from around 50 at 0.2 mM to 10 at 10 mM (see appendix). This decrease of rectification is expected as ionic accumulation and depletion stem from surface effects, which become relatively weaker at high concentration due to higher bulk conductivity [30].

To conclude the pipette characterisation, we measure its conductivity under zero voltage, defined as $G_0 = \mathrm{d}I/\mathrm{d}\Delta V(\Delta V = 0)$, depending on the KCl concentration c (see figure 2(b)). Results show that at high salinity, the conductance is linear with the salt concentration, while it flattens at low concentration due to the surface charge of glass in water [2, 60].

3. Memory spectroscopy

We make a systematic use of the methods introduced in [50, 54] to quantify memory effects. When subjected to time-varying voltage $\Delta V(t) = V_0 \sin(2\pi f t)$, a memristor displays typical I–V characteristics that depend on the driving frequency f. As shown before, the device is a diode at vanishing frequency (figure 2(a)), while it behaves as a resistance at timescales faster than its internal memory time. In intermediate frequency regimes, its I–V curve displays a figure-of-eight, crossing at the origin, which is the hallmark of memristive behaviour. Typical experimental I–V curves are shown in figure 3(a). Both the rectification and the opening of the figure-of-eight depend on the voltage frequency.

For a given set of parameters (KCl concentration c, voltage amplitude ΔV_0), we measure I–V characteristics for various voltage frequencies f and use the area $\mathcal{A}(f)$ of the hysteretic loop to quantify the memory effect. The area $\mathcal{A}(f)$ is defined as

$$\mathcal{A}(f) = -\oint |I(t)| \cdot \mathrm{d}\Delta V(t) \tag{1}$$

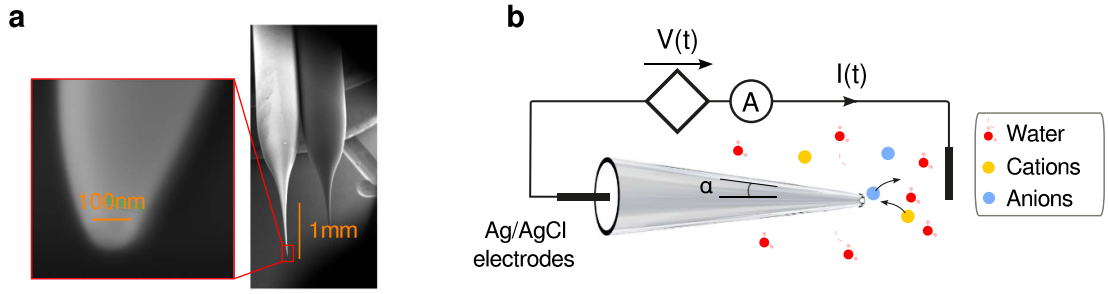

Figure 1. Presentation of the experimental setup. (a) SEM images of glass nanopipettes, with tip radii $R_{\text{tip}} = 50 \pm 15$ nm. The conical pore can be considered as semi-infinite since its geometrical length $L \approx 1$ mm is far greater than any microscopic length. (b) Schematics of the setup for ionic current measurement through the tip of the pipette. Time-varying sinusoidal bias $\Delta V(t) = \Delta V_0 \sin(2\pi f t)$ is imposed between two Ag/AgCl electrodes located inside and outside the nanopipette respectively. The resulting electrical current $I(t)$ is recorded.

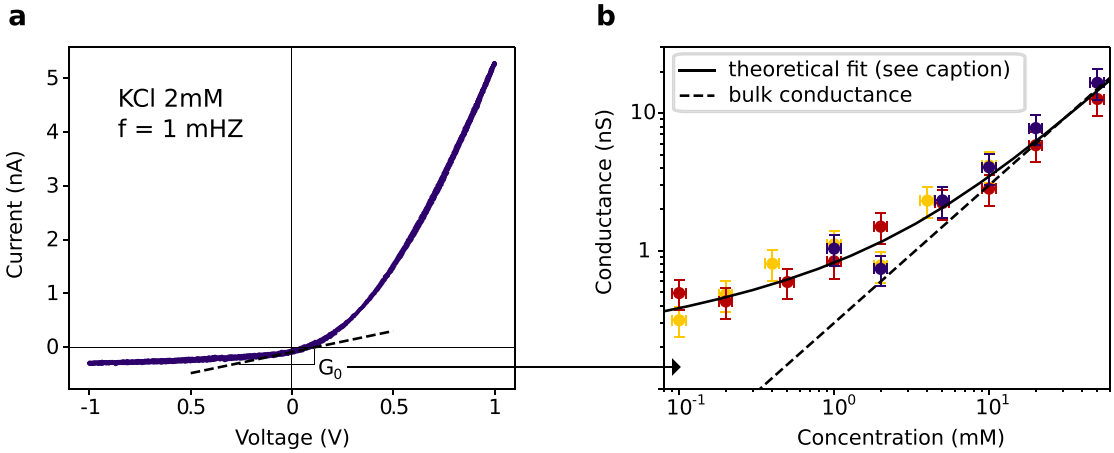

Figure 2. Characterisation of the nanopipettes in low frequency regime. (a) Current–voltage curve of a glass nanopipette in the limit of low frequency ($f = 1$ mHz), where memory effects are negligible. An important current rectification can be observed due to the conical geometry of the channel. The dashed black line represents the conductance at origin $G_0 = \mathrm{d}I/\mathrm{d}\Delta V(\Delta V = 0)$. (b) Conductance $G_0 = \mathrm{d}I/\mathrm{d}\Delta V(\Delta V = 0)$ at zero bias depending on KCl concentration. Three colours represent three distinct nanopipettes. We fit the concentration-dependent conductance with the expression for the conductance of a charged conical nanopore, as derived in the appendix, $G_0 = \mathcal{R}^{-1}$ with $\mathcal{R} = 1/(2\pi\,\alpha\mu e\sigma)\ln(1 + \sigma/(c\mathcal{N}_{\text{A}} e R_{\text{tip}}))$, with the parameters: (half) opening angle $\alpha = 7°$, surface charge $\sigma = 30\,\text{mC}\cdot\text{m}^{-2}$, mobility μ such as $\mu e = 6.7 \cdot 10^{-8}\,\text{m}^2\cdot\text{V}^{-1}\cdot\text{s}^{-1}$, tip radius $R_{\text{tip}} = 55$ nm.

where the integral runs over the voltage cycle. $\mathcal{A}(f)$ has the dimension of a power. To facilitate comparison across frequency and concentration, we further define the normalised $A(f) = \mathcal{A}(f)/(2\Delta V_0 \Delta I(f))$, with $\Delta I(f)$ the difference between maximal and minimal intensities of $\mathcal{A}$ for a given frequency. In what follows, we display only normalised area $A(f)$ rather than its dimensional counterpart. The resulting curve of normalised loop area as function of voltage frequency forms the memory spectrum of the memristor.

4. Double memristive resonance

On figure 3, we plot the memory spectrum of a glass nanopipette at 100 μM KCl concentration. As outlined above, the loop area vanishes in the low and high frequency limits. At intermediate frequencies however, we find that $A(f)$ reaches not one but two maxima $f_{\text{fast}} \approx 3$ Hz and $f_{\text{slow}} \approx 3$ mHz, yielding two timescales over which conductance changes in the channel $\tau_{\text{fast}} \sim 1/2\pi f_{\text{fast}} \sim 50$ ms and $\tau_{\text{slow}} \sim 1/2\pi f_{\text{slow}} \sim 50$ s. We attribute such a large separation in timescales to two distinct transport mechanisms occurring through vastly different kinetics. In particular, while a memory time around 50 ms is consistent with previous findings in glass nanopipettes, a long-term memory has not been reported before in this context.

Then, we investigate how the mem-spectrometry results depend on salt concentration c, which we vary between 10^{-1} and 10^2 mM (see figure 4). On the one hand, we observe that the low frequency peak occurs at $f_{\text{slow}} \approx 3$ mHz irrespective of the electrolyte concentration, but that its amplitude sharply decreases with increasing salt concentration. We plot in figure 5(a) the amplitude of the peak—i.e. the normalised loop area at the frequency f_{slow}—as a function of the salt concentration c. We hypothesise that this long-term memory

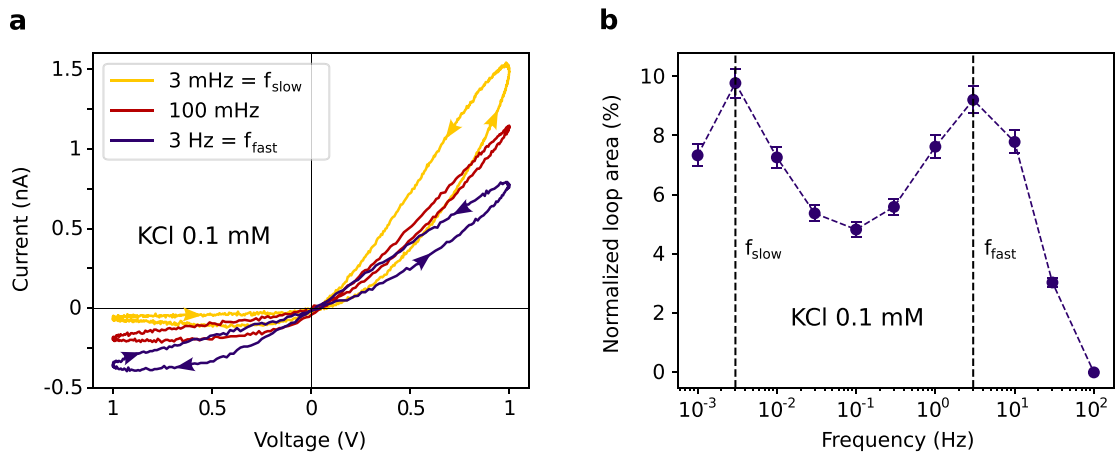

Figure 3. Experimental results of the memory spectrometry carried on a nanopipette at low KCl concentration $c = 0.1$ mM. (a) I–V characteristic of Pipette 1 for low KCl concentration $c = 10^{-4}$ M, and various driving frequencies f: $f_{\text{slow}} = 3$ mHz, $f = 100$ mHz, and $f_{\text{fast}} = 3$ Hz. (b) Results of the memory spectrometry: normalised loop area depending on the bias frequency. Two peaks are highlighted, which shows that significant conductance variations occurs both over long timescales and over short timescales.

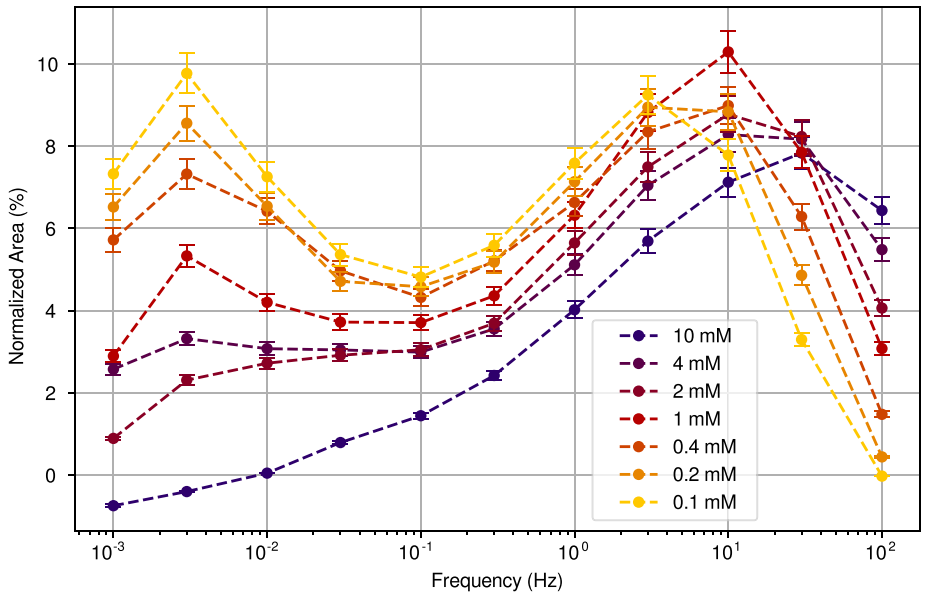

Figure 4. Experimental results: memory spectra for a range of concentrations c, ranging between 10^{-1} and 10^{1} mM.

is associated with surface effects—consistent with the decrease of the relative magnitude of surface conduction at high concentration. In contrast, the high frequency peak amplitude varies remarkably little depending on c, whereas its position on frequency axis increases with concentration. On figure 5(b), we report the scaling of f_{fast} with c for three different pipettes. We see that the short-term memory time roughly follows the scaling $\tau_{\text{fast}} \propto c^{-\chi}$ with $\chi \approx 0.5$. We finally note that these results are robust when changing of nanopipettes, as demonstrated in figure 5. Raw data for the mem-spectrometry curves for various concentrations for various pipettes are further provided in the appendix.

5. Modelling for the dual memristive response

So far, the typical interpretation for the memory time in a nanopore is that the accumulation and depletion of ions should occurs over a typical memory time τ coinciding with the diffusion time of ions through the channel, $\tau \approx L_{\text{eff}}^2/D$, with D the diffusivity of ions and L_{eff} a characteristic length of the channel. Taking $L_{\text{eff}} \sim 10\,\mu$m as the effective nanopipette length—defined so that it accounts for 90% of the overall resistance, (c.f. Appendix A) – and $D = 1.75 \cdot 10^{-9}\,\text{m}^2 \cdot \text{s}^{-1}$, one gets accordingly $\tau \approx 50$ ms in good agreement with the short time scale evidenced in the mem-spectrometry. We note however that the scaling of this time-scale

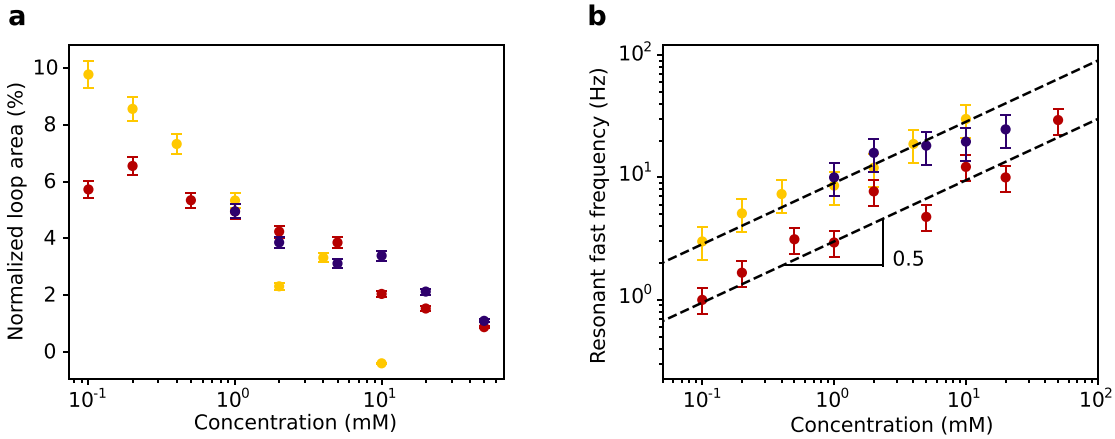

Figure 5. Memory spectrometry: experimental results. (a) Amplitude of the low frequency peak, depending on the electrolyte concentration, for 3 glass nanopipettes, represented with three distinct colours. (b) Dependence of the fast resonant frequency f_{fast} with the ion concentration, for three glass nanopipettes, represented with three distinct colours.

with the salt concentration, as reported in figure 5(b), matches the dependence of the Debye length λ_D. This may suggest that the fast time is related to an RC time-scale, with $\tau_{RC} \sim \lambda_D L/D$ for the charging dynamics between 2 electrodes. Quantitatively however, this would yield a memory time of the order of a few microseconds, far below the experimentally measured value for the fast time-scale. One would need to introduce an arbitrarly large prefactor, which would therefore contain most of the physics. We therefore argue that the fast time scale is diffusive, with the scaling $\tau \sim L^2/D$, as was furthermore supported by previous analytical and experimental work on conical nanopores by Kamsma *et al* [49]. Hence, we assume that the short-term memory in our pipettes—associated with the memory peak at f_{fast}—stems from diffusive dynamics.

Now, the source for the long-term memory, i.e. the peak at f_{slow}, is less clear. The surface charge carried by the nanopipette wall is a natural candidate for slow internal relaxation. A first indication is that the slow frequency peak drops as concentration increases, hence as the contribution of surface conduction becomes negligible as compared to its bulk counterpart. Furthermore, it is known that the surface charge on a nanochannel wall depends on salt concentration and pH [8, 61] and recent works showed that this may induce some peculiar and very slow relaxation dynamics, due e.g. to flow recirculations in presence of inhomogeneous surface charge relaxation processes [62, 63].

In the following, we propose a simple modelling accounting for both the non-linear (frequency-dependent) I–V curves and the emergence of memory effects in charged conical nanopore. A specificity of the conical geometry is that it behaves as an ionic diode, as evidenced here again in figure 2 and any modelling has to account for this non-linear transport behaviour. The latter is a signature of the complex ion dynamics inside the asymmetric channel, akin a P–N junction. In principle, describing the dynamics of ions in our nanopipettes would require to solve the 3D Poisson–Nernst–Planck equations in a conical geometry. This was done in the steady state in [30, 38, 39], while the kinetics were investigated only for infinitesimal time-dependent voltage drops in [56].

Here our objective is to built a simplified modelling on the basis of the gross features of the mechanisms at play. A key point is the asymmetric transport of anions (co-ions) and cations (counter-ions), due to the presence of a (negative) surface charge. A voltage drops results, at the tip, from an increased transference of cations and a suppressed transference of anions [30, 38]. This asymmetry in the partitioning of the ionic transport between surface and bulk then leads to an accumulation/depletion of ions occurs near the tip [20, 21, 30]. This concentration polarisation at the tip is at the origin of the non-linear response. This will occur as the Dukhin length, defined in terms of the local ion concentration c and surface charge σ as $\ell_{\text{Du}} = \frac{\sigma}{\mathcal{N}_A e c}$, is larger than the tip radius R_{tip}. Equivalently the Dukhin number (defined here at the tip) $\text{Du}_{\text{in}} = \frac{\sigma}{R_{\text{tip}} \mathcal{N}_A e c_{\text{in}}}$ is larger than unity. Accordingly, the modelling has to account for the kinetics of ionic accumulation and depletion near the tip of the nanopipette. This is what we propose here.

We model the glass pipette as a a conical pore of length $L_{\text{eff}} \approx 10\,\mu$m, placed between two reservoirs at concentration c_{ext}, as sketched on figure 6(a). The pore has a tip radius $R_{\text{tip}} = 55$ nm, opening half angle $\alpha = 7°$, base radius $R_{\text{base}} = \alpha L_{\text{eff}}$ and volume of interest $\mathcal{V} = \pi L_{\text{eff}} R_{\text{base}}^2/3$, with a constant surface charge σ on its walls. We assume $\sigma \sim -30\,\text{mC}\cdot\text{m}^{-2}$.

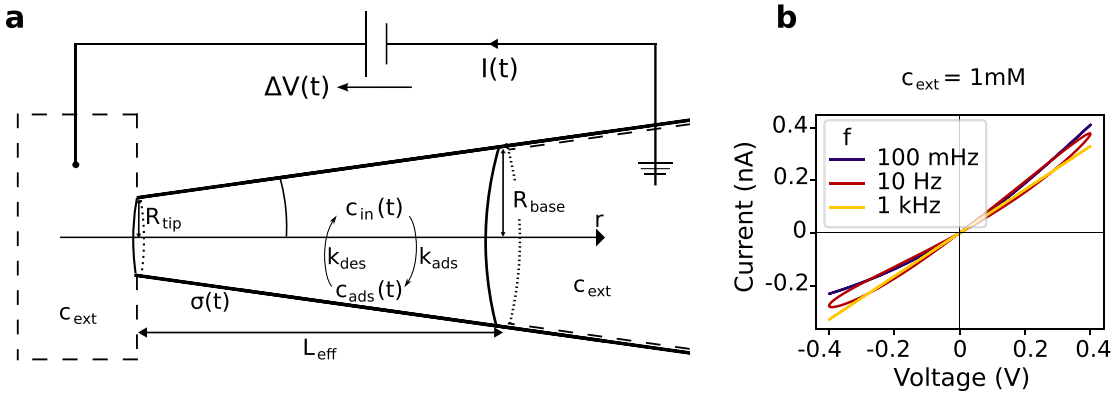

Figure 6. Schemes for the various models introduced (see text for details). (a) Scheme of the geometry and the flux of the conical nanopore. (b) Results for the I–V characteristics with Model 0, for voltage amplitude $\Delta V_0 = 400$ mV, frequency $f = 1$ mHz, and concentration $c_{\rm ext} = 1$ mM.

To describe the voltage-dependent memristive response of the pipettes, we use a two- or three-states model, which separates the ion profiles into homogeneous populations in separate regions: in the channel, in the reservoirs and on the surfaces [54, 64]. The concentration in the reservoirs (outside of the nanopipette) is fixed to $c_{\rm ext}$, while the concentration takes a different value $c_{\rm in}$ near the tip of the nanopipette, as a result from the time-dependent accumulation and depletion (Model 0). Ions can also be present at the surface in the form of a time-dependent surface charge $\sigma(t)$ (Model 1) or as an adsorbed specie with concentration $c_{\rm ads}$ (Model 2). The surface charge and surface conduction induce an asymmetry in the current response to ΔV which, depending on its sign, either increases or lowers the inner concentration $c_{\rm in}$.

We now describe the various models based on these assumptions.

5.1. Model 0: Ion transport in a charged conical pore

In the most simplified modelling, we describe the kinetics of the inner concentration $c_{\rm in}$ in terms of the competition between the ionic transport leading to concentration accumulation/depletion at the tip and the various processes which would relax the concentration gradient in the tip. We assume for now that the surface charge σ is fixed.

As stated above, the accumulation/depletion of ions occurs near the tip occurs due to the asymmetric ionic transport under the electric field. Note that deviations to electroneutrality can be neglected because it is short-lived with respect to memory timescales. The corresponding electrophoretic transport is therefore at the origin of the concentration contrast between the inner and outer concentration and this is modelled as a generic flux $\gamma\Delta V$, with γ a coefficient accounting for the voltage induced concentration gradients. An estimate for γ in terms of accumulation of ions is discussed in the appendix B, yielding $\gamma \sim (2e\mathcal{N}_{\rm A}\mathcal{V}\mathcal{R})^{-1}$.

Such concentration gradients will then be relaxed by diffusion and electro-osmosis, which both tend to relax $c_{\rm in}$ back to $c_{\rm ext}$. The diffusion flux from inside to outside the pore is of the order $D\,\pi R_{\rm base}^2/L_{\rm eff}\times(c_{\rm in}-c_{\rm ext})$, where $L_{\rm eff}$ is the typical length over which the concentration varies and $\pi R_{\rm base}^2$ is the area of the exchange surface. On the other hand, the voltage drop ΔV induces an electro-osmotic flow of amplitude $|Q| = S_{\rm stm}|\Delta V|$, with $S_{\rm stm}$ the streaming conductance of the pore. This flow $|Q|$ is responsible for a flux of the order of $|Q|\,(c_{\rm in}-c_{\rm ext})$. Altogether, the relaxation flux behaves as $-(c_{\rm in}-c_{\rm ext})/\tau(\Delta V)$ with the typical time associated with concentration relaxation accounting for the two previous relaxation mechanisms:

$$\tau(\Delta V) = \frac{\mathcal{V}}{\pi\alpha^2 D L_{\rm eff} + |\Delta V S_{\rm stm}|} = \left(\frac{1}{\tau_{\rm Diff}} + \frac{1}{\tau_{\rm EO}(\Delta V)}\right)^{-1} \tag{2}$$

with $\tau_{\rm Diff} = \mathcal{V}/\pi\alpha^2 D L_{\rm eff} \approx L_{\rm eff}^2/3D$ the typical diffusion timescale, and $\tau_{\rm EO}(\Delta V) = \mathcal{V}/|\Delta V S_{\rm stm}|$ the timescale of concentration relaxation due to electro-osmosis.

Gathering the different contributions, one can thus write a simple dynamics for $c_{\rm in}$ in the form

$$\frac{\partial c_{\rm in}}{\partial t} = \gamma\Delta V - \frac{1}{\tau(\Delta V)}(c_{\rm in}-c_{\rm ext}) \tag{3}$$

where $\tau(\Delta V)$ the concentration relaxation time. Note that we do not include time-nonlocal effects in the modelling of the dynamics, merely for simplicity. A time-local model where parameters can be physically

estimated allows for simpler interpretations. Then, we solve the time-dependent equation (3) to obtain the time-dependent concentration of the pore $c_{\rm in}(t)$. Once the pore concentration is known, the ionic current in the system is then obtained as

$$I(t) = \frac{1}{\mathcal{R}(t)} \times \Delta V(t) \tag{4}$$

according to Ohm's law. Here $\mathcal{R}$ is the ionic resistance of the nanopipette, the expression of which is obtained in the appendix A as

$$\mathcal{R}(t) = \frac{1}{2\pi\,\alpha\mu e\sigma} \ln\left(1 + \frac{\ell_{\rm Du}\left[c_{\rm in}(t)\right]}{R_{\rm tip}}\right) \tag{5}$$

with the ion mobility μ such as $\mu e = 6.7 \cdot 10^{-8}\,\mathrm{m^2 \cdot s^{-1} \cdot V^{-1}}$, and $\ell_{\rm Du}[c_{\rm in}]$ is the Dukhin length defined in terms of the inner concentration $c_{\rm in}$.

In the stationary state under a constant voltage drop ΔV, equation (3) accounts for the inner concentration $c_{\rm in}(\Delta V) = c_{\rm ext} + \gamma\tau(\Delta V) \times \Delta V$ which depends on the applied voltage. After inserting $c_{\rm in}(\Delta V)$ into equation (5) and computing equation (4), one obtains the I–V curve of a diode, asymmetric in the voltage reversal, $\Delta V \to -\Delta V$.

Let us now solve equation (3) under an AC sinusoidal bias, $\Delta V(t) = \Delta V_0 \sin(2\pi f t)$ to obtain the time-dependent concentration $c_{\rm in}(t)$ and then the corresponding current $I(t)$. In the following, we use typically $\Delta V_0 = 400$ mV (which is small enough to ensure that $|c_{\rm in} - c_{\rm ext}| < c_{\rm ext}$ at any time t) and $S_{\rm stm} = 0.1\,\mathrm{nA \cdot bar^{-1}}$. We report the I–V characteristics for various frequencies and $c_{\rm ext} = 1$ mM in figure 6(b). As shown on this figure, the model predicts indeed a current rectification with the emergence of a memory for intermediate frequencies (here $f \sim 10$ Hz). This behaviour is in agreement with the experimental result, see figure 3(a). Now, calculating the memory using the same descriptor as in the experiments, equation (1), one obtains the full memory spectrometry predicted by this model, see figure 7(b). As highlighted on this figure, Model 0 exhibits indeed a frequency-dependent memory effect, with a single, but broad, memory peak at relatively 'high' frequency $f \approx 10$ Hz. As expected, the value for the peak frequency is close to $f \approx (\tau_{\rm Diff})^{-1} + (\tau_{\rm EO}(\Delta V_0))^{-1} \sim 10$ Hz.

Therefore, Model 0 accounts for the current rectification and the high frequency memory, but it does not capture the slow memory effects.

5.2. Model 1: Surface charge regulation

In a refined model, we thus add the dynamics of surface charging as an supplementary dynamical process. First, in contrast to Model 0 where the surface charge σ was assumed to be constant, we introduce here its dependence on the local concentration $c_{\rm in}$ in the tip. This is expected, as the surface charge of glass in water is known to depend on the local ionic strength and pH [8, 60]. Second, we assume that the surface charge σ relaxes exponentially over a slow time scale τ_σ :

$$\frac{\mathrm{d}\sigma}{\mathrm{d}t} = -\frac{1}{\tau_\sigma}\left[\sigma - \sigma_\infty(c_{\rm in})\right] \tag{6}$$

where $\sigma_\infty(c_{\rm in})$ accounts for the (equilibrium) surface charge regulation as a function of the local salt concentration. Then, we assume a scaling relationship between surface charge and concentration, as:

$$\sigma_\infty(c_{\rm in}) = \left(\frac{c_{\rm in}}{c_0}\right)^{\beta} \sigma_0 \tag{7}$$

where $\sigma_0 = -30\mathrm{mC \cdot m^{-2}}$ is the surface charge at low concentration $c_0 = 0.1$ mM. In the following, we will consider $\beta \simeq 0.33$, as observed in carbon nanotubes and predicted using a Poisson–Boltzmann theory [8].

The coupled dynamics for the tip concentration and the surface charge are solved numerically under an AC voltage driving, $\Delta V(t) = \Delta V_0 \sin(2\pi f t)$, following the same procedure as above. Results for the frequency dependent memory are reported in figure 7(c). Model 1 indeed reproduces the existence of two well-separated memory peaks, at high and low frequency values. To account for the experimental value of the slow memory frequency, one needs to assume a very long charge relaxation time τ_σ, here $\tau_\sigma = 50$ s. Although this value seems extremely long as compared to any expected diffusive and adsorption time-scales in the system, it is interesting to note that similarly long relaxations were evidenced in the charging dynamics of electrified surfaces (there, CaF2) [62, 63, 65]. Interestingly, the model also qualitatively predicts the vanishing of the long-term memory effects at high salt concentration. Overall, the regulation of surface charge by salt concentration is a plausible origin of the reported long-term memory.

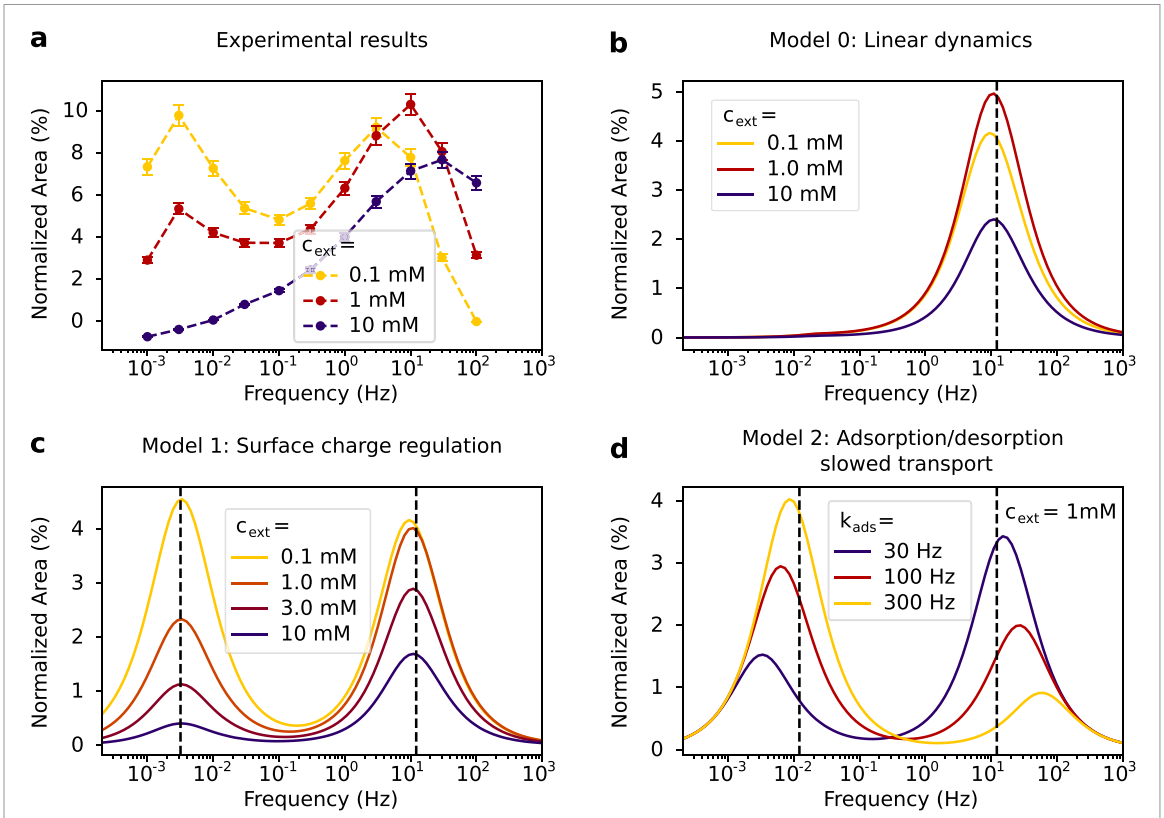

Figure 7. Mem-spectrometry predicted by the various models. (a) Experimental memory spectrometry on a glass nanopipette at several ions concentrations. (b) Memory spectrometry predicted by Model 0 with varying parameter c_{ext} and $\Delta V_0 = 400$ mV. Black dashed line labels $f_{fast} = (\pi \alpha^2 D L_{eff} + \Delta V_0 S_{stm})/(2\pi \mathcal{V})$; (c) Memory spectroscopy predicted by Model 1, with $\tau_\sigma = 50$ s, exponent $\beta = 1/3$, $\Delta V_0 = 400$ mV and varying c_{ext}. Black dashed lines label $f_{slow} = 1/2\pi\tau_\sigma$ and $f_{fast} = (\pi \alpha^2 D L_{eff} + \Delta V_0 S_{stm})/(2\pi \mathcal{V})$. (d) Memory spectroscopy predicted by Model 2 with $\Delta V_0 = 400$ mV, varying k_{ads} and keeping the ratio $k_{ads}/k_{des} = 1000$. Black dashed lines label $f_{fast} = (\pi \alpha^2 D L_{eff} + \Delta V_0 S_{stm})/(2\pi \mathcal{V})$ and $f_{slow} = f_{fast} \cdot k_{des}/k_{ads}$.

5.3. Model 2: Surface-adsorption hindered transport

While Model 1, based on the (ultra-slow) surface charging dynamics is able to account for the general features of the memory spectrum, one may propose alternative models, based on the 'adsorption/desorption' dynamics of the ions on the channel wall, e.g. in the Stern layer at the surface. Such an hypothesis was indeed proposed in [54] to account for long memory timescales (of the order of ≈ 100 s) in 2D nanochannels, inconsistent with diffusion timescale. The authors postulated that ions could not diffuse freely in the channel, but rather spent long period of time adsorbed at the channel wall. We explore this model here as an alternative scenario.

In order to simplify the description, we assume a fixed surface charge as in Model 0 (with $\sigma = -30\,\mathrm{mC}\cdot\mathrm{m}^{-2}$), but consider that ions can be adsorbed at and desorbed from the wall. The adsorbed ions, at concentration c_{ads}, do not contribute to the pipette conductance. Denoting the adsorption rate k_{ads} and desorption at rate k_{des}, we thus describe the kinetics in terms of the two coupled equations for c_{in} and c_{ads}

$$\frac{\partial c_{in}}{\partial t} = \gamma \Delta V - \frac{1}{\tau(\Delta V)}(c_{in} - c_{ext}) - k_{ads} c_{in} + k_{des} c_{ads} \tag{8}$$

$$\frac{\partial c_{ads}}{\partial t} = k_{ads} c_{in} - k_{des} c_{ads}. \tag{9}$$

As proposed in [54], if $k_{ads} \gg k_{des}$, most ions are adsorbed. The adsorption sites play the role of a reservoir, and increase the time necessary to fill the pipette tip by a factor k_{ads}/k_{des}, thus slowing down the dynamics by the same factor. This model is solved numerically under an AC voltage driving, $\Delta V(t) = \Delta V_0 \sin(2\pi f t)$, and we report in figure 7(d) the mem-spectrometry as a function of the imposed frequency f, for various values of the parameter k_{ads}, while the ratio k_{ads}/k_{des} is fixed to $k_{ads}/k_{des} = 10^3$. As shown on figure 7(d), this adsorption/desorption model accounts for the emergence of two memory timescales. For $k_{ads} \gg f_{fast} = 1/2\pi\tau$, c_{ads} is always at equilibrium with c_{in}. On the other hand, for $k_{ads} \ll f_{fast}$, c_{ads} remains almost constant over τ_{fast} when c_{in} varies. In both these limiting cases, the diffusive origin to memory (Model 0) dominates, yielding a single peak. In the intermediate range where k_{ads} compares with $1/\tau$, two memory peaks are observed.

These results show that the long-term memory is cancelled at low k_{ads}. Accordingly the concentration dependence of the low frequency peak observed in the experiments, see figure 7(a), could be accounted for by assuming that the adsorption rate k_{ads} is a function of salt concentration.

This model is solved numerically under an AC voltage driving, $\Delta V(t) = \Delta V_0 \sin(2\pi f t)$, and we report in figure 7(d) the mem-spectrometry as a function of the imposed frequency f, for various values of the parameter k_{ads}, while the ratio k_{ads}/k_{des} is fixed to $k_{ads}/k_{des} = 10^3$. As shown on figure 7(d), this adsorption/desorption model accounts for the emergence of two memory timescales. In the limiting case $k_{ads} \gg f_{fast} = 1/2\pi\tau$, as proposed in [54], the adsorption sites play the role of a reservoir, and increase the time necessary to fill the pipette tip by a factor k_{ads}/k_{des}, thus slowing down the dynamics by the same factor. Accordingly, as shown in figure 6(d), for high values of k_{ads}, the memory spectrometry displays a resonance at low frequency $f_{slow} = f_{fast} \cdot k_{des}/k_{ads}$. On the other hand, for $k_{ads} \ll f_{fast}$, c_{ads} remains almost constant over τ_{fast} when c_{in} varies. We thus recover the dynamics of Model 0, with a short-term memory. Finally, in the intermediate range where k_{ads} compares with $1/2\pi\tau$, two memory peaks are observed.

These results show that the long-term memory is cancelled at low k_{ads}. Accordingly the concentration dependence of the low frequency peak observed in the experiments, see figure 7(a), could be accounted for by assuming that the adsorption rate k_{ads} is a function of salt concentration.

6. Discussion and conclusion

The main results of this work is the experimental demonstration of two characteristic memory times and their dependencies with the ionic concentration in glass nanopipettes. We have shown that a simple modelling of the kinetics of concentration polarisation is able to capture not only the ionic rectification but also the emergence of various memory effects. The key ingredient is a bias-induced concentration polarisation near the tip of the asymmetric channel, caused by the interplay of the conical geometry with surface transport. That such a simplistic description, with only very few ingredients, is able to account for the complex non-linear kinetics is already a successful outcome of the approach. However, some features of the experimental results are only partly reproduced, such as the concentration dependence of the fast resonance frequency.

Furthermore, to explain the low frequency peak, one has to assume the existence of long relaxation times for the surface processes, be it surface charging or ion adsorption (Model 1 and 2). For example, in Model 1, the surface-charge regulation model assumes a notably long typical time $\tau_\sigma \sim 50$ s. Such timescale cannot originate only from an activated chemical process, such as silanol deprotonation, the latter being a exothermic, activationless process [66]. Now, as mentioned above, memory effects occurring over thousands of seconds were evidenced in previous experiments, such as in reference [65], and attributed to surface charge regulation of the CaF_2 substrate, with the diffusion of hydronium limiting the kinetics of the regulation. Another mechanism giving rise to slow dynamics was proposed in [67], involving divalent and trivalent anions, which we are not expected to play a role here.

On the other hand, Model 2, based on the adsorption/desorption model allows long timescales to arise from the coupling of two (faster) dynamics, as long as their ratio is large enough $k_{ads}/k_{des} \gg 1$. The adsorption/desorption dynamics featured in this model was hypothesised to play a major role in ion transport in 2D nanochannels under high confinement [54], and noise measurements supported the existence of this phenomenon [64]. Since this dynamics gives rise to either short-term or long-term memory depending on the comparison between k_{ads} and $1/\tau_{fast}$, our work suggests that short- or long-term memory can be tuned by modifying the nanochannel length L, or modifying the diffusion coefficient of ions for example. Actually, the measured 'fast' memory time of 50 ms is indeed quite long for iontronic applications (although it is of the same order of magnitude as the opening/closing times of many voltage-gated biological channels, 10–100 ms). This time-scale could be shortened by reducing the length of the nanopores. Alternatively, advection inside the pore could accelerate the relaxation dynamics.

In order to go beyond, one should develop a full PNP model of the nanopipette, in the spirit of [39, 56, 63], accounting not only for the various kinetic effects—diffusion, electro-osmosis and -phoresis, etc –, but also for the concentration polarisation and its consequence on transport non-linearities. We leave such exhaustive study for future work.

The charged conical nanopores presented here belong to the class of nanofluidic memristors relying on concentration modulation induced by voltage drops. Hebbian learning [54], reservoir computing [49] were already demonstrated in such memristors. Moreover, theoretical work predicted that such devices could be used in spiking circuits [52, 56, 68]. We demonstrate here the existence of long timescales that only play significant role at low ion concentration, and coexist with short timescales, is of broad practical interest for iontronics applications to the neuromorphic computing. Indeed, such long memory memristors can keep track in their internal state of data submitted in the past and take them into account them to process new

submitted data. It can be interpreted in term of short-term plasticity and long-term potentiation/depression, a pair of mechanisms which are crucial for the learning process in biological brains.

Besides iontronics, our work relates to any situation involving confined electrolytes and time-varying voltage, e.g. semi-permeable membranes for water desalination or osmotic energy conversion. Mem-spectroscopy is shown to be a powerful tool to understand the entangled ionic dynamics taking place in nanofluidic devices.

Data availability statement

All data that support the findings of this study are included within the article (and any supplementary files).

Acknowledgments

The authors acknowledge ERC n-AQUA for funding. S J acknowledges CNRS for funding. The authors thank Hummink for pipette supply and characterization. P R acknowledges funding from the European Union Horizon 2020 research and innovation program under the Marie Skodowska-Curie Grant Agreement No. 101034413.

Appendix A. Conductance of a semi-infinite charged conical nanopore

We consider the semi-infinite charged conical nanopore with tip radius $R_{\rm tip}$, ion concentration c and opening half angle α, parametrised with the radial distance r to the cone tip, as shown in figure 7. The distance r_0 is accordingly defined in terms of the pipette opening $R_{\rm tip}$ as $r_0 = R_{\rm tip}/\tan\alpha$.

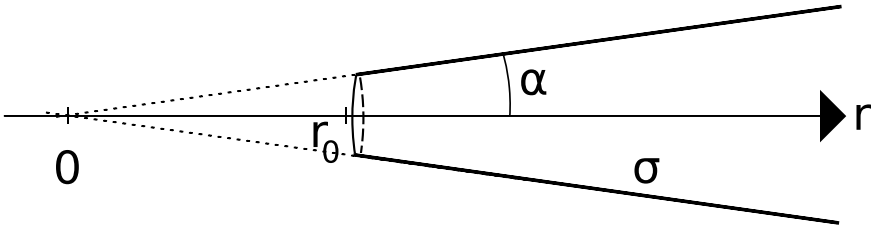

Figure 8. Schematics of a conical pipette tip. The distance r is taken from the cone tip.

In the absence of surface conduction, the 'bulk' resistance writes

$$\mathcal{R}_{\rm bulk} = \int_{r_0}^{\infty} \frac{{\rm d}r}{2\Omega r^2 \mu \mathcal{N}_{\rm A} e^2 c} = \frac{1}{2\Omega r_0 \mu \mathcal{N}_{\rm A} e^2 c}, \tag{10}$$

with $\Omega = 2\pi\,(1-\cos(\alpha))$ the solid angle, μ the mobility of ions, $\mathcal{N}_{\rm A}$ the Avogadro number, and e the elementary charge. In the limit of small α, one gets

$$\mathcal{R}_{\rm bulk} \simeq \frac{1}{2\pi\alpha R_{\rm tip} \mu \mathcal{N}_{\rm A} e^2 c}. \tag{11}$$

Note that this corresponds to the resistance of a cylindrical channel with radius $R_{\rm tip}$ and effective length $\approx R_{\rm tip}/\alpha$.

Now in the presence of a surface charge σ on the walls of the nanopipette, the resistance of a infinitesimal layer of radial distance r is

$${\rm d}\mathcal{R} = \frac{{\rm d}r}{2\pi\tan(\alpha)\, r\mu e\sigma + 2\Omega r^2 \mu \mathcal{N}_{\rm A} e^2 c}. \tag{12}$$

The resistance of the portion between r_0 and a maximal distance r_1 is

$$\mathcal{R} = \int_{r_0}^{r_1} \frac{{\rm d}r}{2\pi\tan(\alpha)\, r\mu e\sigma + 2\Omega r^2 \mu \mathcal{N}_{\rm A} e^2 c} = \frac{1}{2\Omega\mu\mathcal{N}_{\rm A} e^2 c} \times \frac{1}{\ell}\int_{r_0}^{r_1} {\rm d}r \left(\frac{1}{r} - \frac{1}{r+\ell}\right) \tag{13}$$

with $\ell = \frac{\pi \tan(\alpha)\sigma}{\Omega \mathcal{N}_A e c}$. One gets

$$\mathcal{R} = \frac{1}{2\pi \tan(\alpha)\mu e \sigma}\left[\ln\left(\frac{r_1}{r_1+\ell}\right) - \ln\left(\frac{r_0}{r_0+\ell}\right)\right]. \tag{14}$$

Considering $r_1 \to \infty$ and $\alpha \to 0$, one gets the total resistance as

$$\mathcal{R} \simeq \frac{1}{2\pi\,\alpha\mu e\sigma}\ln\left(1+\frac{\ell_{\mathrm{Du}}}{R_{\mathrm{tip}}}\right) \tag{15}$$

where $\ell_{\mathrm{Du}} = \alpha\ell = \frac{\sigma}{\mathcal{N}_A e c}$ is a Dukhin length (assuming a small opening angle α).

As a final note, one can estimate an effective length L_{eff} of the nanopipette in terms of the length $L_{\mathrm{eff}} = r_1 - r_0$ such that the corresponding resistance $\mathcal{R}(r_1)$ in equation (14) is a coefficient 90% of the total resistance in equation (15) for $r_1 \to \infty$. Using equation (14), this leads to the expression for $L_{\mathrm{eff}} = \frac{\ell}{(1+\ell/r_0)^{1-\gamma}-1} - r_0$, with $\ell = \ell_{\mathrm{Du}}/\alpha$, $r_0 = R_{\mathrm{tip}}/\alpha$ and $\gamma = 0.9$ (90%). Typically, for $c = 1$ mM, $\sigma = 30\,\mathrm{mC\,m^{-2}}$, one gets a value $L_{\mathrm{eff}} \approx 10\,\mu$m.

Appendix B. Concentration polarisation under voltage drop and estimate of the γ parameter

The parameter γ defines the rate at which average inside concentration c_{in} deviates away from c_{ext} under a voltage drop ΔV. It is defined as the (electrophoretic) flux of ions towards the tip under the voltage drop

$$\left.\frac{\partial c_{\mathrm{in}}}{\partial t}\right|_{EP} = \gamma \Delta V. \tag{16}$$

To estimate its numerical value, we assume that the electrical current $I(t) = \Delta V(t)/\mathcal{R}(t)$ entering the pore is equal to the current leaving the pore, so the pore remains quasi electro-neutral at all time t. We then proceed to count the number of co- and counter-ions entering and leaving the pore, in a way similar to [56]. Defining $\mathrm{Du_{tip}}$ and $\mathrm{Du_{base}}$ the Dukhin number at the tip and the base of the conical pore respectively, the current at the base of the cone is carried by a fraction $1/[2(1+\mathrm{Du_{base}})]$ of co-ions and a fraction $(1+2\mathrm{Du_{base}})/[2(1+\mathrm{Du_{base}})]$ of counter-ions, while the current at the tip of the cone is carried by a fraction $1/[2(1+\mathrm{Du_{tip}})]$ of co-ions and a fraction $(1+2\mathrm{Du_{tip}})/[2(1+\mathrm{Du_{tip}})]$ of counter-ions (see figure 6(b)). Hence a number

$$\mathrm{d}t \cdot I(t) \cdot \frac{1}{2\mathcal{N}_A e}\left(\frac{1}{1+\mathrm{Du_{base}}} - \frac{1}{1+\mathrm{Du_{tip}}}\right)$$

of co-ions accumulate inside the pore during dt (and an equal number of counter-ions). Altogether,

$$\left.\frac{\partial c_{\mathrm{in}}}{\partial t}\right|_{EP} = \left[\frac{1}{1+\mathrm{Du_{base}}} - \frac{1}{1+\mathrm{Du_{tip}}}\right] \cdot \frac{1}{2\mathcal{R}\mathcal{V}\mathcal{N}_A e} \cdot \Delta V(t)\,.$$

This rough estimation allow us to get a numerical estimate for the parameter γ in our model: $\gamma = [1/(1+\mathrm{Du_{base}}) - 1/(1+\mathrm{Du_{tip}})]/(2\mathcal{R}\mathcal{V})$. For the estimation of the Dukhin numbers and resistance $\mathcal{R}$ we consider $c_{\mathrm{in}} \approx c_{\mathrm{ext}}$, thus γ does not depend on c_{in}. Again, this approximation is valid for small enough ΔV.

For low Dukhin number $\mathrm{Du_{tip}} \ll 1$, on e gets $\gamma \approx \pi\,\mu\alpha e\sigma$ $\gamma \approx \pi\,\mu\alpha\sigma/\mathcal{N}_A\mathcal{V}$, coinciding with the expression from [56], while at high Dukhin number $\mathrm{Du_{base}} \gg 1$, $\gamma \approx \pi\,\mu\alpha e^2\mathcal{N}_A c R_{\mathrm{base}}$ $\gamma \approx \pi\,\mu e\alpha c R_{\mathrm{base}}/\mathcal{V}$, with no dependence with σ. This can be understood in term of minority charge carrier transport limitation: at low Dukhin number, the excess surface conductance giving rise to the concentration variation is limiting compared to the bulk conductance, while at high Dukhin number, the ion concentration variation is limited by the bulk current to preserve electroneutrality.

In the nanopipette and the concentration under scrutiny, $\mathrm{Du_{base}} \ll 1 < \mathrm{Du_{tip}}$, so that

$$\gamma \approx \frac{1}{2\mathcal{N}_A e \mathcal{R}\mathcal{V}}. \tag{17}$$

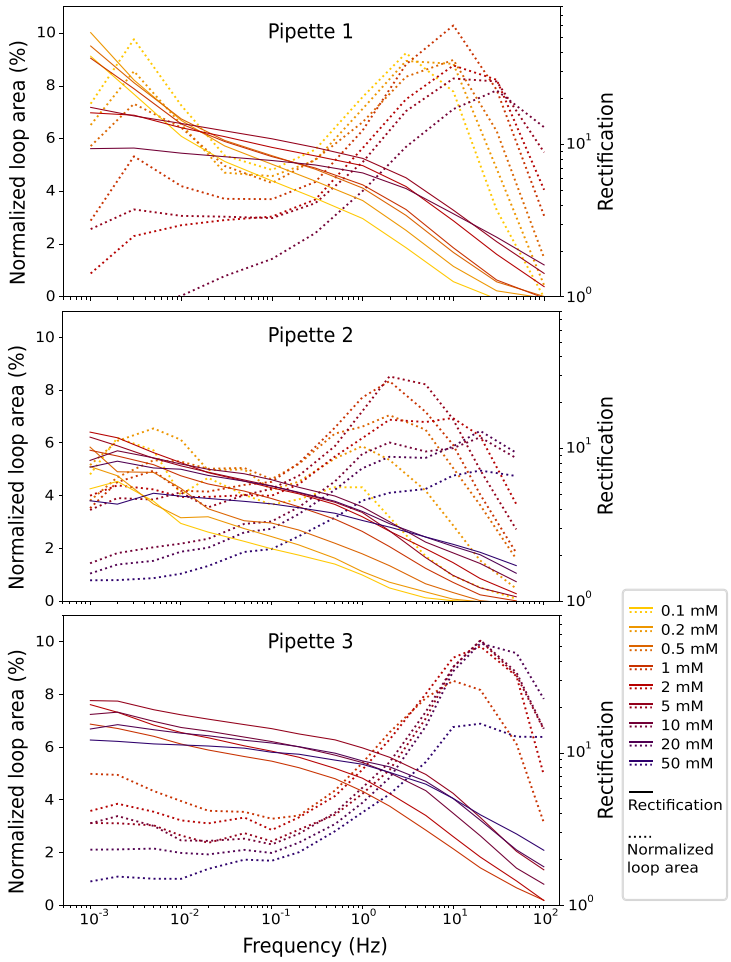

Figure 9. Memory spectrometry carried on three pipettes, and variations of the rectification ration with the frequency. Rectification decreases with frequency while the loop area is non monotonous.

Appendix C. Detailed memory spectrometry and rectification depending on salt concentration for three pipettes

We provide in figure S3 the memory spectrometries at several salt concentration for the three glass nanopipettes we used, with same tip radius $R_{\text{tip}} = 50 \pm 15$ nm. The three pipettes exhibit qualitatively the same behaviour: the short-term memory peak shifts toward the higher frequencies at higher salt concentration, while and the low frequency peak vanishes. We also display the rectification of the pipettes depending on the AC voltage frequency, defining the rectification as the ratio $I(\Delta V = 1\text{V})/I(\Delta V = -1\text{V})$. As expected, the rectification ratio decreases with the frequency, and the normalised area peaks coincide with sharp rectification variations.

References

[1] Schoch R B, Han J and Renaud P 2008 Transport phenomena in nanofluidics *Rev. Mod. Phys.* **80** 839–83
[2] Bocquet L and Charlaix E 2010 Nanofluidics, from bulk to interfaces *Chem. Soc. Rev.* **39** 1073–95
[3] Kavokine N, Netz R R and Bocquet L 2021 Fluids at the nanoscale: from continuum to subcontinuum transport *Annu. Rev. Fluid Mech.* **53** 377–410
[4] Stein D, Kruithof M and Dekker C 2004 Surface-charge-governed ion transport in nanofluidic channels *Phys. Rev. Lett.* **93** 035901
[5] Schoch R B, van Lintel H and Renaud P 2005 Effect of the surface charge on ion transport through nanoslits *Phys. Fluids* **17** 100604
[6] Duan C and Majumdar A 2010 Anomalous ion transport in 2-nm hydrophilic nanochannels *Nat. Nanotechnol.* **5** 848
[7] Siria A, Poncharal P, Biance A-L, Fulcrand R, Blase X, Purcell S T and Bocquet L 2013 Giant osmotic energy conversion measured in a single transmembrane boron nitride nanotube *Nature* **494** 455–8
[8] Secchi E, Nigues A, Jubin L, Siria A and Bocquet L 2016 Scaling behavior for ionic transport and its fluctuations in individual carbon nanotubes *Phys. Rev. Lett.* **116** 154501
[9] Emmerich T, Vasu K S, Niguès A, Keerthi A, Radha B, Siria A and Bocquet L 2022 Enhanced nanofluidic transport in activated carbon nanoconduits *Nat. Mater.* **21** 696
[10] Vlassiouk I, Smirnov S and Siwy Z 2008 Ionic selectivity of single nanochannels *Nano Lett.* **8** 1978–85

[11] Yossifon G, Mushenheim P, Chang Y-C and Chang H-C 2009 Nonlinear current-voltage characteristics of nanochannels *Phys. Rev. E* **79** 046305
[12] Perera R T, Johnson R P, Edwards M A and White H S 2015 Effect of the electric double layer on the activation energy of ion transport in conical nanopores *J. Phys. Chem.* **119** 24299–306
[13] Esfandiar A, Radha B, Wang F C, Yang Q, Hu S, Garaj S, Nair R R, Geim A K and Gopinadhan K 2017 Size effect in ion transport through angstrom-scale slits *Science* **358** 511–3
[14] Gopinadhan K, Hu S, Esfandiar A, Lozada-Hidalgo M, Wang F C, Yang Q, Tyurnina A V, Keerthi A, Radha B and Geim A K 2019 Complete steric exclusion of ions and proton transport through confined monolayer water *Science* **363** 145–8
[15] Wei C and Bard A 1997 Current rectification at quartz nanopipet electrodes *Anal. Chem.* **69** 4627–4233
[16] Apel P, Korchev Y, Siwy Z, Spohr R and Yoshida M 2001 Diode-like single-ion track membrane prepared by electro-stopping *Nucl. Instrum. Methods Phys. Res. B* **184** 337–46
[17] Siwy Z and Fuliński A 2002 Fabrication of a synthetic nanopore ion pump *Phys. Rev. Lett.* **89** 198103
[18] Woermann D 2002 Analysis of non-ohmic electrical current-voltage characteristic of membranes carrying a single track-etched conical pore *Nucl. Instrum. Methods Phys. Res. B* **194** 458–62
[19] Siwy Z, Dobrev D, Neumann R, Trautmann C and Voss K 2003 Electro-responsive asymmetric nanopores in polyimide with stable ion-current signal *Appl. Phys. A* **76** 781–5
[20] Siwy Z, Heins E, Harrell C C, Kohli P and Martin C R 2004 Conical-nanotube ion-current rectifiers: the role of surface charge *J. Am. Chem. Soc.* **126** 10850
[21] Woermann D 2003 Electrochemical transport properties of a cone-shaped nanopore: high and low electrical conductivity states depending on the sign of an applied electrical potential difference *Phys. Chem. Chem. Phys.* **5** 1853–8
[22] Cheng L-J and Guo L J 2007 Rectified ion transport through concentration gradient in homogeneous silica nanochannels *Nano Lett.* **7** 3165–71
[23] Vlassiouk I and Siwy Z S 2007 Nanofluidic diode *Nano Lett.* **7** 552–6
[24] Vlassiouk I, Smirnov S and Siwy Z 2008 Nanofluidic ionic diodes. Comparison of analytical and numerical solutions *ACS Nano* **2** 1589–602
[25] Kovarik M L, Zhou K and Jacobson S C 2009 Effect of conical nanopore diameter on ion current rectification *J. Phys. Chem. B* **113** 15960
[26] Yossifon G, Chang Y-C and Chang H-C 2009 Rectification, gating voltage and interchannel communication of nanoslot arrays due to asymmetric entrance space charge polarization *Phys. Rev. Lett.* **103** 154502
[27] Ai Y, Zhang M, Joo S W, Cheney M A and Qian S 2010 Effects of electroosmotic flow on ionic current rectification in conical nanopores *J. Phys. Chem.* **114** 3883–90
[28] Green Y, Edri Y and Yossifon G 2015 Asymmetry-induced electric current rectification in permselective systems *Phys. Rev. E* **92** 033018
[29] Xiong T, Zhang K, Jiang Y, Yu P and Mao L 2019 Ion current rectification: from nanoscale to microscale *Sci. China Chem.* **62** 1346–59
[30] Poggioli A R, Siria A and Bocquet L 2019 Beyond the tradeoff: dynamic selectivity in ionic transport and current rectification *J. Phys. Chem. B* **123** 1171
[31] Aarts M, Boon W Q, Cuenod B, Dijkstra M, van Roij R and Alarcon-Llado E 2022 Ion current rectification and long-range interference in conical silicon micropores *ACS Appl. Mater. Interfaces* **14** 56226–36
[32] Powell M R, Sullivan M, Vlassiouk I, Constantin D, Sudre O, Martens C C, Eisenberg R S and Siwy Z S 2007 Nanoprecipitation-assisted ion current oscillations *Nat. Nanotechnol.* **3** 51–57
[33] Innes L, Powell M R, Vlassiouk I, Martens C and Siwy Z S 2010 Precipitation-induced voltage-dependent ion current fluctuations in conical nanopores *J. Phys. Chem.* **114** 8126–34
[34] Vilozny B, Actis P, Seger R A and Pourmand N 2011 Dynamic control of nanoprecipitation in a nanopipette *ACS Nano* **5** 3191–7
[35] Lan W-J, Holden D A and White H S 2011 Pressure-dependent ion current rectification in conical-shaped glass nanopores *J. Am. Chem. Soc.* **133** 13300–3
[36] Luo L, Holden D A, Lan W-J and White H S 2012 Tunable negative differential electrolyte resistance in a conical nanopore in glass *ACS Nano* **6** 6507–14
[37] Luo L, Holden D A and White H S 2014 Negative differential electrolyte resistance in a solid-state nanopore resulting from electroosmotic flow bistability *ACS Nano* **8** 3023–30
[38] Jubin L, Poggioli A, Siria A and Bocquet L 2018 Dramatic pressure-sensitive ion conduction in conical nanopores *Proc. Natl Acad. Sci. USA* **115** 4063
[39] Boon W Q, Veenstra T E, Dijkstra M and van Roij R 2022 Pressure-sensitive ion conduction in a conical channel: optimal pressure and geometry *Phys. Fluids* **34** 101701
[40] Yamamoto K, Ota N and Tanaka Y 2020 Nanofluidic devices and applications for biological analyses *Anal. Chem.* **93** 332–49
[41] Karhanek M, Kemp J T, Pourmand N, Davis R W and Webb C D 2005 Single DNA molecule detection using nanopipettes and nanoparticles *Nano Lett.* **5** 403–7
[42] Noy A and Darling S B 2023 Nanofluidic computing makes a splash *Science* **379** 143–4
[43] Emmerich T, Teng Y, Ronceray N, Lopriore E, Chiesa R, Chernev A, Artemov V, Di Ventra M, Kis A and Radenovic A 2024 Nanofluidic logic with mechano-ionic memristive switches *Nat. Electron.* **7** 271–8
[44] Daiguji H, Oka Y and Shirono K 2005 Nanofluidic diode and bipolar transistor *Nano Lett.* **5** 2274–80
[45] Karnik R, Fan R, Yue M, Li D, Yang P and Majumdar A 2005 Electrostatic control of ions and molecules in nanofluidic transistors *Nano Lett.* **5** 943–8
[46] Guan W, Fan R and Reed M A 2011 Field-effect reconfigurable nanofluidic ionic diodes *Nat. Commun.* **2** 506
[47] Mohamed E, Josten S and Marlow F 2022 A purely ionic voltage effect soft triode *Phys. Chem. Chem. Phys.* **24** 8311–20
[48] Mohamed E, Tchorz N and Marlow F 2023 Iontronic memories based on ionic redox systems: operation protocols *Faraday Discuss.* **246** 296–306
[49] Kamsma T M, Kim J, Kim K, Boon W Q, Spitoni C, Park J and van Roij R 2024 Brain-inspired computing with fluidic iontronic nanochannels *Proc. Natl Acad. Sci.* **121** e2320242121
[50] Wang D, Brown W, Li Y, Kvetny M, Liu J and Wang G 2018 Hysteresis charges in the dynamic enrichment and depletion of ions in single conical nanopores *ChemElectroChem* **5** 3089–95
[51] Zhang P *et al* 2019 Nanochannel-based transport in an interfacial memristor can emulate the analog weight modulation of synapses *Nano Lett.* **19** 4279–86

[52] Robin P, Kavokine N and Bocquet L 2021 Modeling of emergent memory and voltage spiking in ionic transport through angstrom-scale slits *Science* **373** 687
[53] Brown W, Kvetny M, Yang R and Wang G 2022 Selective ion enrichment and charge storage through transport hysteresis in conical nanopipettes *J. Phys. Chem.* **126** 10872–9
[54] Robin P *et al* 2023 Long-term memory and synapse-like dynamics in two-dimensional nanofluidic channels *Science* **379** 161–7
[55] Xiong T *et al* 2023 Neuromorphic functions with a polyelectrolyte-confined fluidic memristor *Science* **379** 156
[56] Kamsma T M, Boon W Q, ter Rele T, Spitoni C and van Roij R 2023 Iontronic neuromorphic signaling with conical microfluidic memristors *Phys. Rev. Lett.* **130** 268401
[57] Cervera J, Portillo S, Ramirez P and Mafe S 2024 Modeling of memory effects in nanofluidic diodes *Phys. Fluids* **36** 047129
[58] Barnaveli A, Kamsma T, Boon W and van Roij R 2024 Pressure-gated microfluidic memristor for pulsatile information processing *Phys. Rev. Appl.* **22** 054057
[59] Ramirez P, Gomez V, Cervera J, Mafe S and Bisquert J 2023 Synaptical tunability of multipore nanofluidic memristors *J. Phys. Chem. Lett.* **14** 10930–4
[60] Iler R 1979 *The Chemistry of Silica: Solubility, Polymerization, Colloid and Surface Properties and Biochemistry* (Wiley)
[61] Biesheuvel P M and Bazant M Z 2016 Analysis of ionic conductance of carbon nanotubes *Phys. Rev. E* **94** 050601(R)
[62] Lis D, Backus E H G, Hunger J, Parekh S H and Bonn M 2014 Liquid flow along a solid surface reversibly alters interfacial chemistry *Science* **344** 1138–42
[63] Ober P, Boon W Q, Dijkstra M, Backus E H G, van Roij R and Bonn M 2021 Author correction: liquid flow reversibly creates a macroscopic surface charge gradient *Nat. Commun.* **12** 6987
[64] Robin P, Lizee M, Yang Q, Emmerich T, Siria A and Bocquet L 2023 Disentangling 1/f noise from confined ion dynamics *Faraday Discuss.* **246** 556–75
[65] Wang Y, Seki T, Gkoupidenis P, Chen Y, Nagata Y and Bonn M 2024 Aqueous chemimemristor based on proton-permeable graphene membranes *Proc. Natl Acad. Sci.* **121** e2314347121
[66] Lowe B M, Skylaris C-K and Green N G 2015 Acid-base dissociation mechanisms and energetics at the silica-water interface: an activationless process *J. Colloid Interface Sci.* **451** 231–44
[67] Kamsma T, Klop M, Boon W, Spitoni C, Rueckauer B and van Roij R 2025 Chemically regulated conical channel synapse for neuromorphic and sensing applications *Phys. Rev. Res.* **7** 013328
[68] Kamsma T, van Roij R and Spitoni C 2024 A simple mathematical theory for simple volatile memristors and their spiking circuits *Chaos Solitons Fractals* **186** 115320